

Supporting information

Core-shell nanoporous AuCu₃@Au monolithic electrode for efficient electrochemical CO₂ reduction

Xiaoming Ma^{a†}, Yongli Shen^{a†}, Shuang Yao^a, Cuihua An^a, Weiqing Zhang^{a,*}, Junfa Zhu^c, Rui Si^{b,*}, Chunxian Guo^d, and Changhua An^{a,*}

^aTianjin Key Laboratory of Organic Solar Cells and Photochemical Conversion, School of Chemistry and Chemical Engineering and Tianjin Key Laboratory of Advanced Functional Porous Materials, Institute for New Energy Materials & Low-Carbon Technologies, Tianjin University of Technology, Tianjin 300384, P. R. China

E-mail: anch@tjut.edu.cn

^b Shanghai Synchrotron Radiation Facility, Shanghai Institute of Applied Physics, Chinese Academy of Sciences, Shanghai, 201204 China

E-mail: sirui@sinap.ac.cn

^cNational Synchrotron Radiation Laboratory, University of Science and Technology of China, Hefei, Anhui 230029, People's Republic of China

^d Institute for Advanced Materials and Devices, Suzhou University of Science and Technology, Suzhou 215009, China

The calculation of faradaic efficiency (FE):

$$FE(\%) = \frac{N_{CO}}{N_{total}} \times 100\%$$

$$N_{CO} = x_0 \times \frac{P \times V_0}{R \times T} \times N_A \times 2e$$

$$N_{total} = \frac{I_0 \times \frac{V_0}{\vartheta}}{e}$$

Where:

V_0 = the volume of the sample loop for hydrocarbons in our gas chromatograph (1 cm³)

v = the flow rate of the gas = 10 cm³ / min

x_0 (ppm) = the number of electrons (CO) needed

I_0 (mA) = steady-state cell current

$P = 1.013 \times 10^5$ Pa, $R = 8.314$ J·K⁻¹·mol⁻¹, $T = 299.15$ K, $N_A = 6.02 \times 10^{23}$ mol⁻¹,

$e = 1.602 \times 10^{-19}$ C/e

Each test was repeated 3 times to guarantee the consistency.

The ECSA can be calculated from the equation:

$$A_{ECSA} = \frac{\text{Specific capacitance}}{40 \mu F \text{ cm}^{-2} \text{cm}_{ECSA}^{-2}}$$

The specific capacitance can be converted into an ECSA using the specific capacitance value for a flat standard with 1 cm² of real surface area. For most metallic and semiconducting materials in the same aqueous electrolyte, their specific capacitance for a flat surface is generally found to be in the range of 20-60 µF cm⁻².¹ Here we assume 40 µF cm⁻² as a moderate value for nanoporous Au and AuCu₃@Au.²

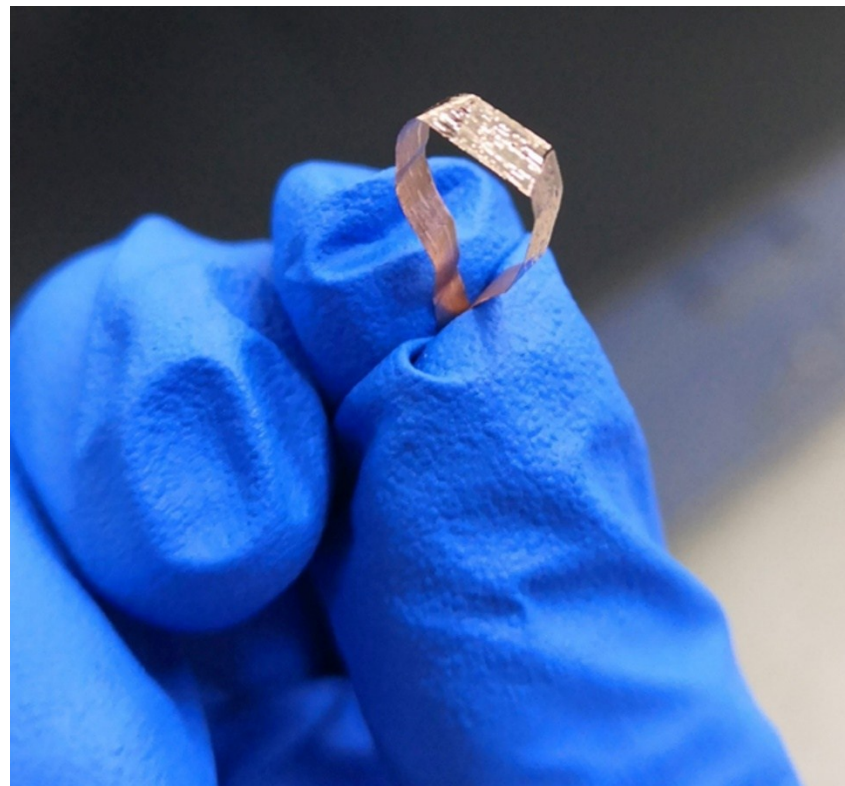


Fig. S1. A picture of flexible bulk nanoporous alloys of $\text{AuCu}_3@\text{Au}$.



Fig. S2. A photograph of the obtained flexible bulk nanoporous $\text{AuCu}_3@\text{Au}$ electrode.

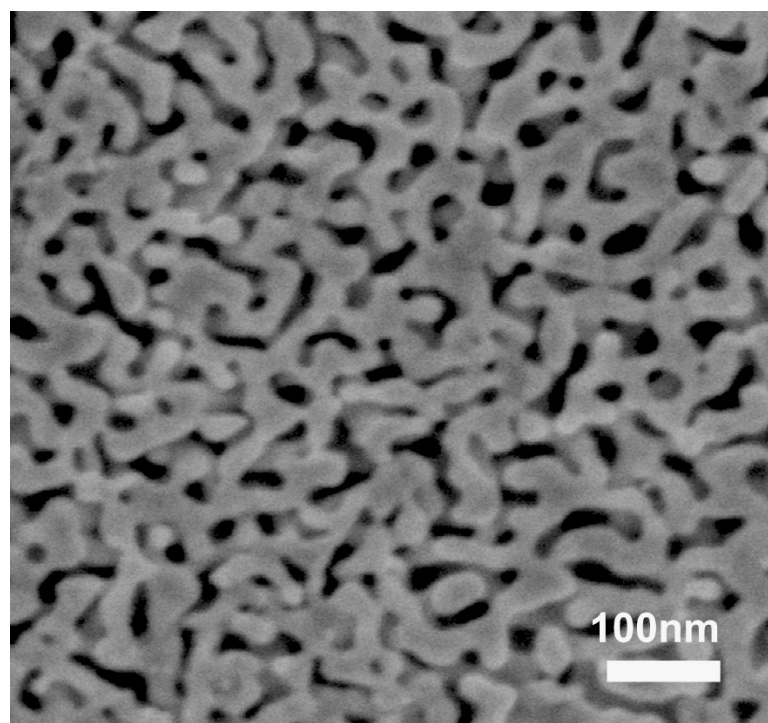


Fig. S3. An SEM image of monolithic $\text{AuCu}_3@\text{Au}$ nanoporous electrode.

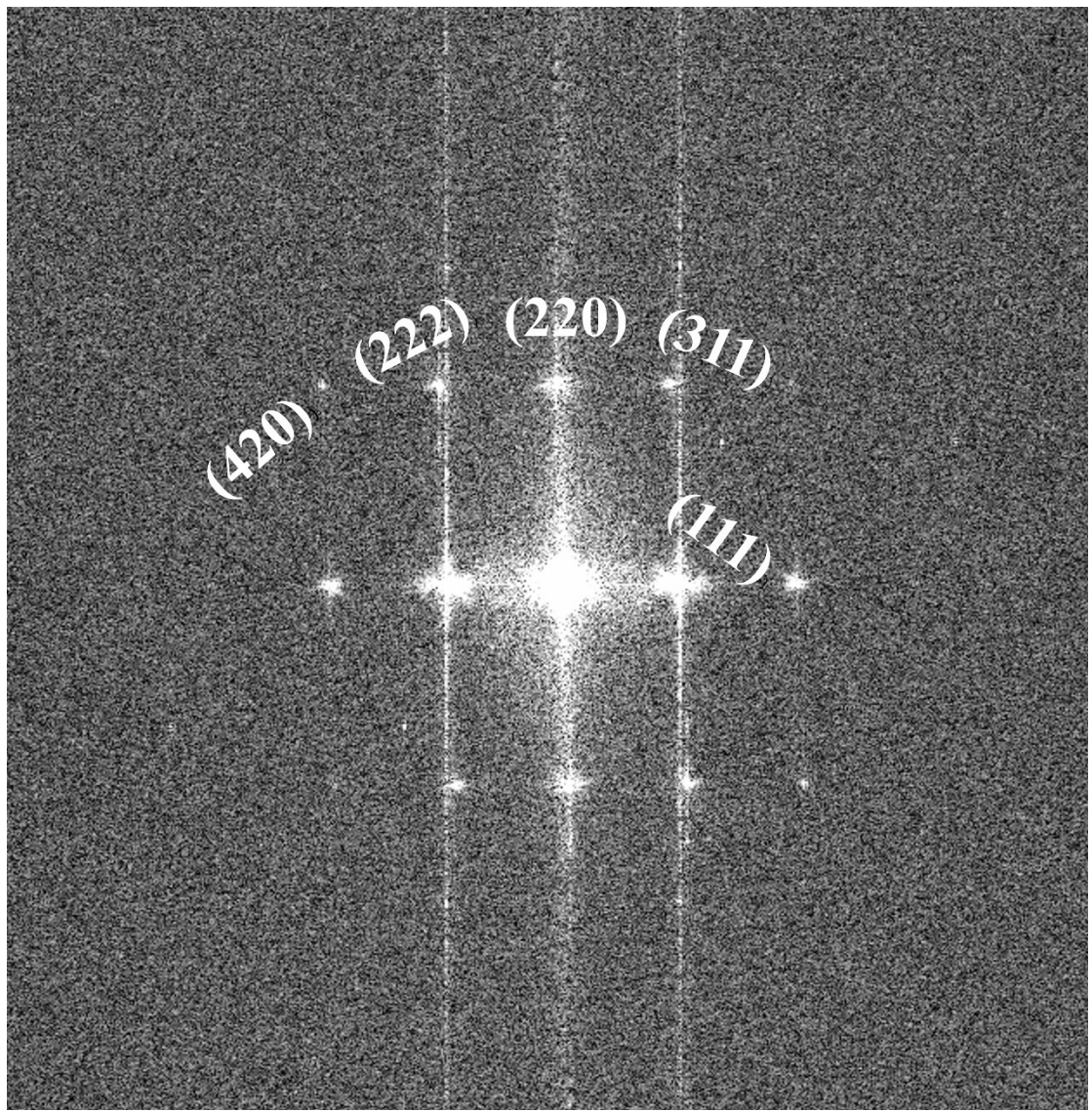


Fig. S4. Fast Fourier transform (FFT) pattern of Figure 1e.

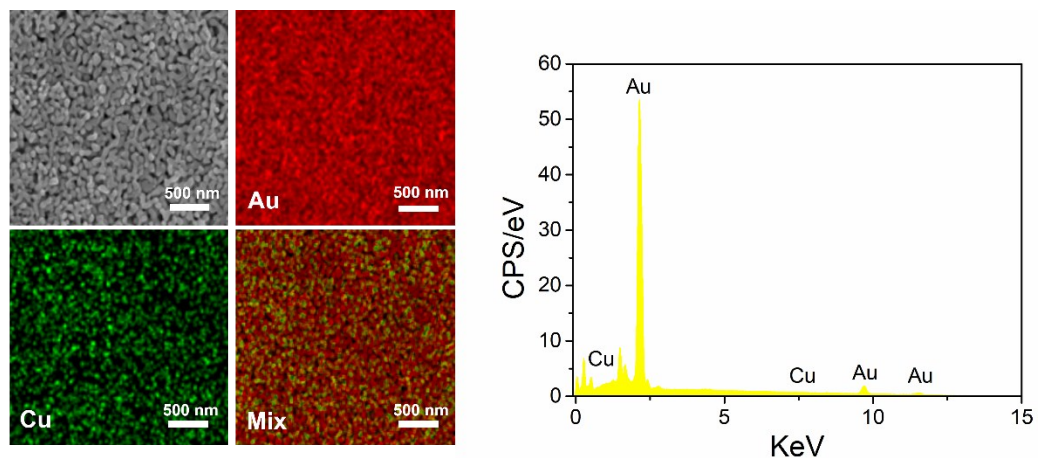


Fig.S5. SEM-EDS elemental mapping of nanoporous $\text{AuCu}_3@\text{Au}$.

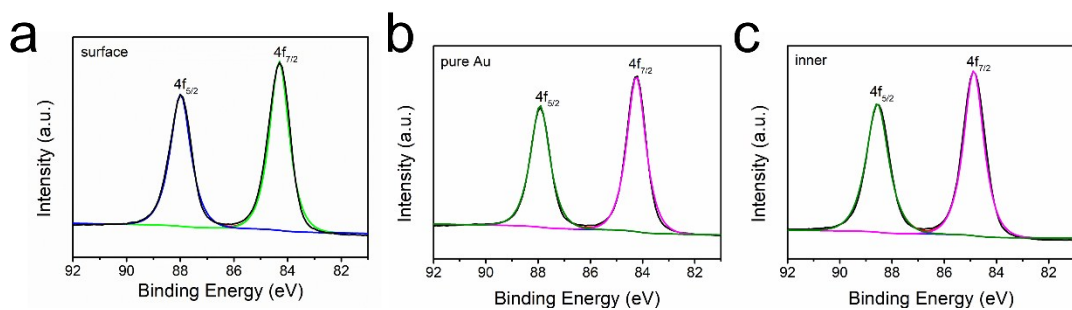


Fig. S6. XPS of Au 4f. (a) surface Au over nanoporous $\text{AuCu}_3@\text{Au}$, (b) pure Au, (c) inner Au of nanoporous $\text{AuCu}_3@\text{Au}$.

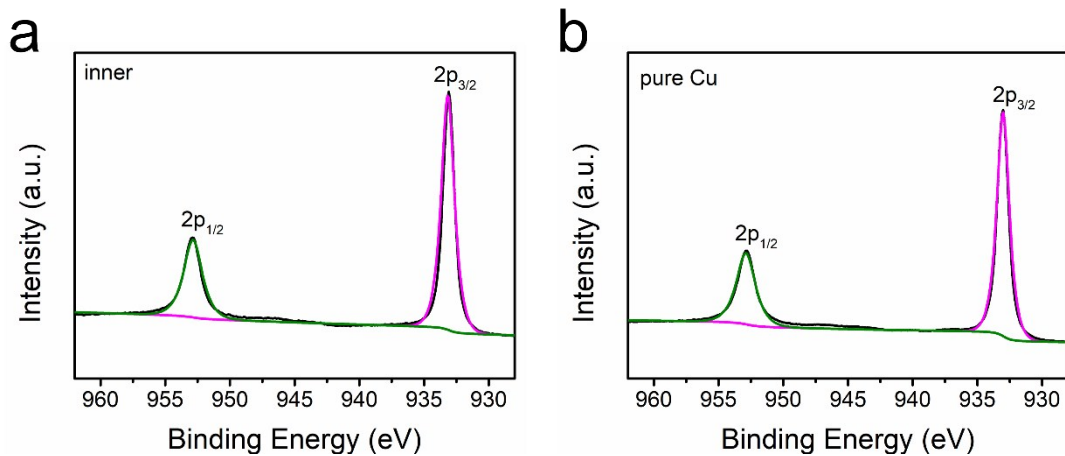


Fig. S7. XPS of Cu 2p. (a) inner Cu in nanoporous $\text{AuCu}_3@\text{Au}$; (b) pure Cu.

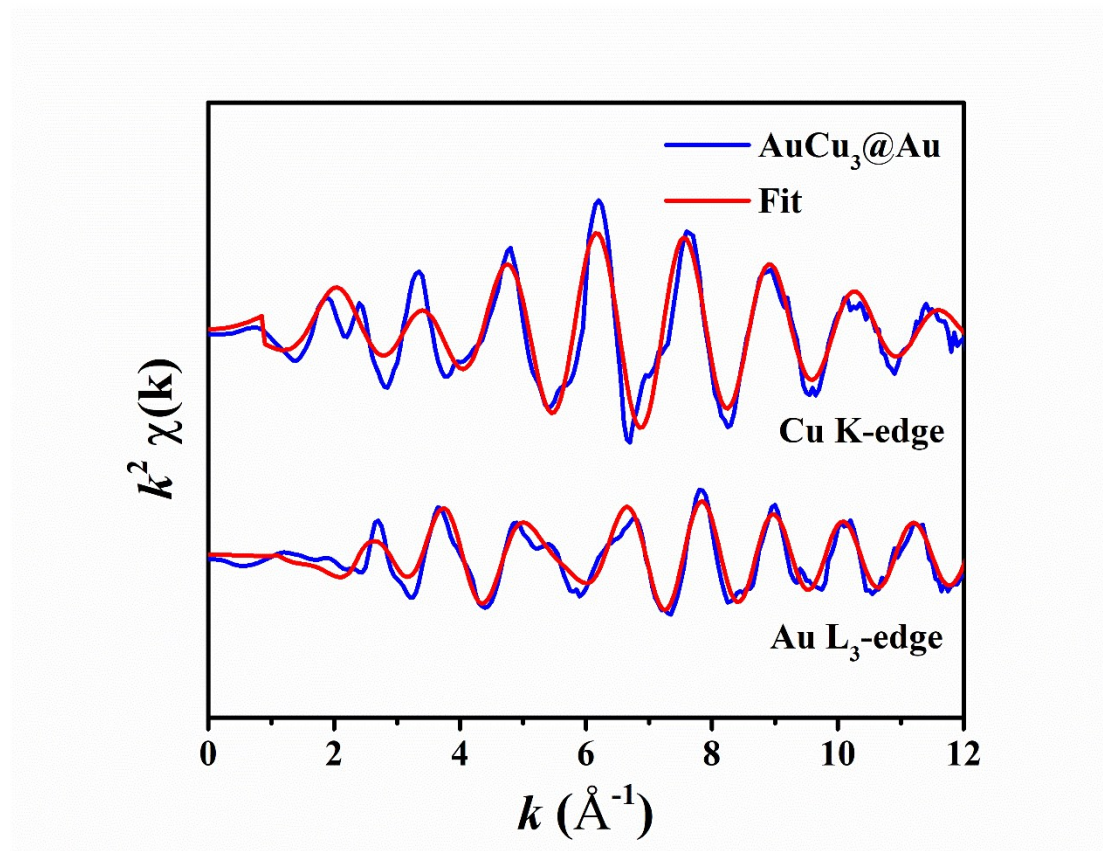


Fig. S8. k-space data of nanoporous $\text{AuCu}_3@\text{Au}$ for Au L₃-edge and Cu K-edge.

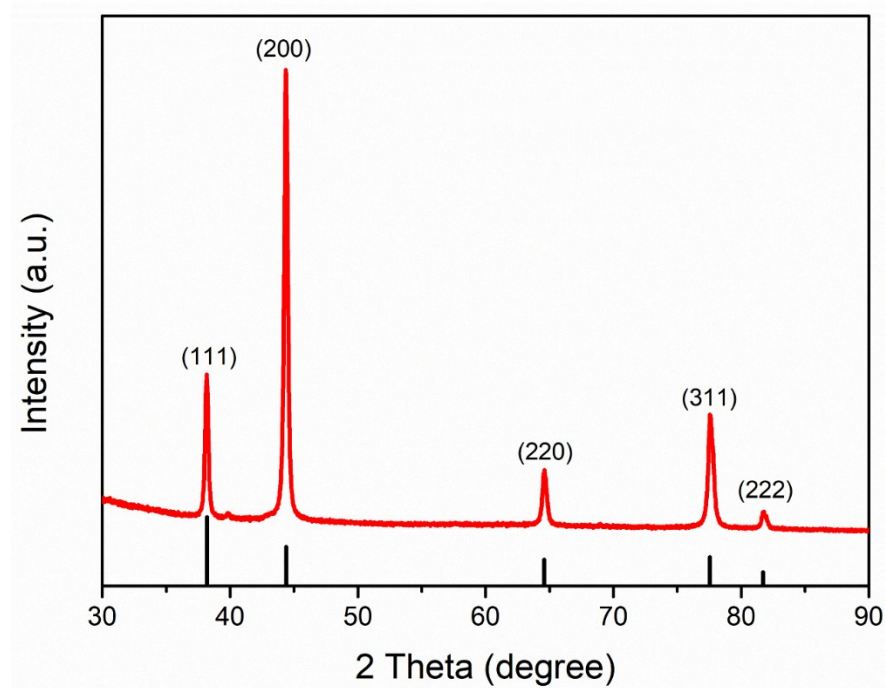


Fig. S9. XRD pattern of nanoporous Au with a standard one highlighted by chopsticks.

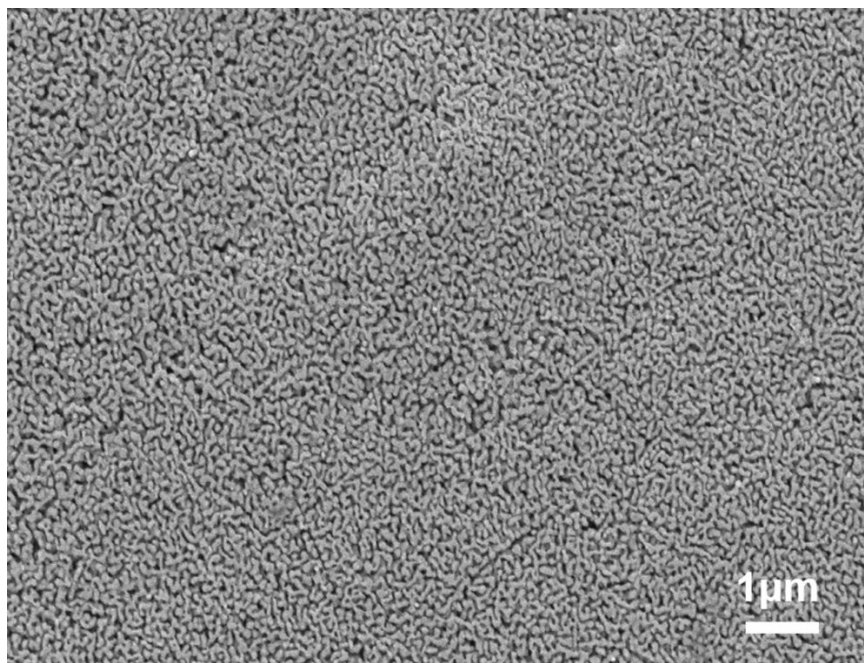


Fig. S10. An SEM image of nanoporous Au.

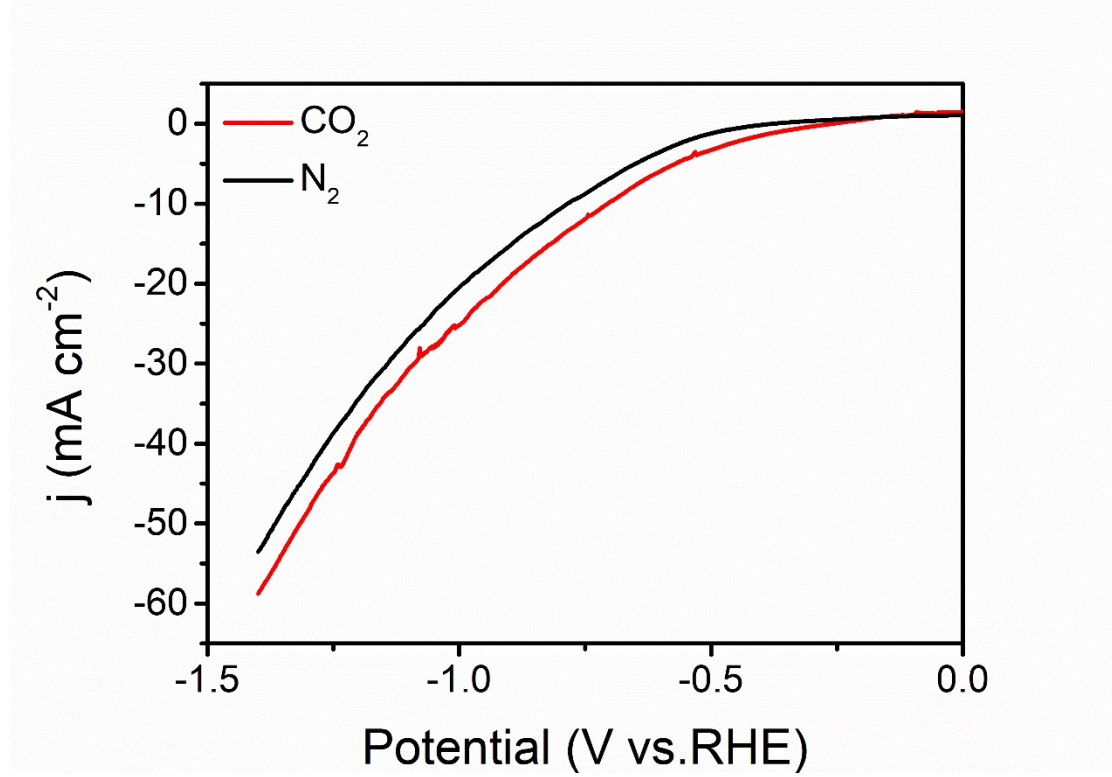


Fig. S11. LSV curves in N_2 and CO_2 -saturated 0.1M KHCO_3 over nanoporous Au.

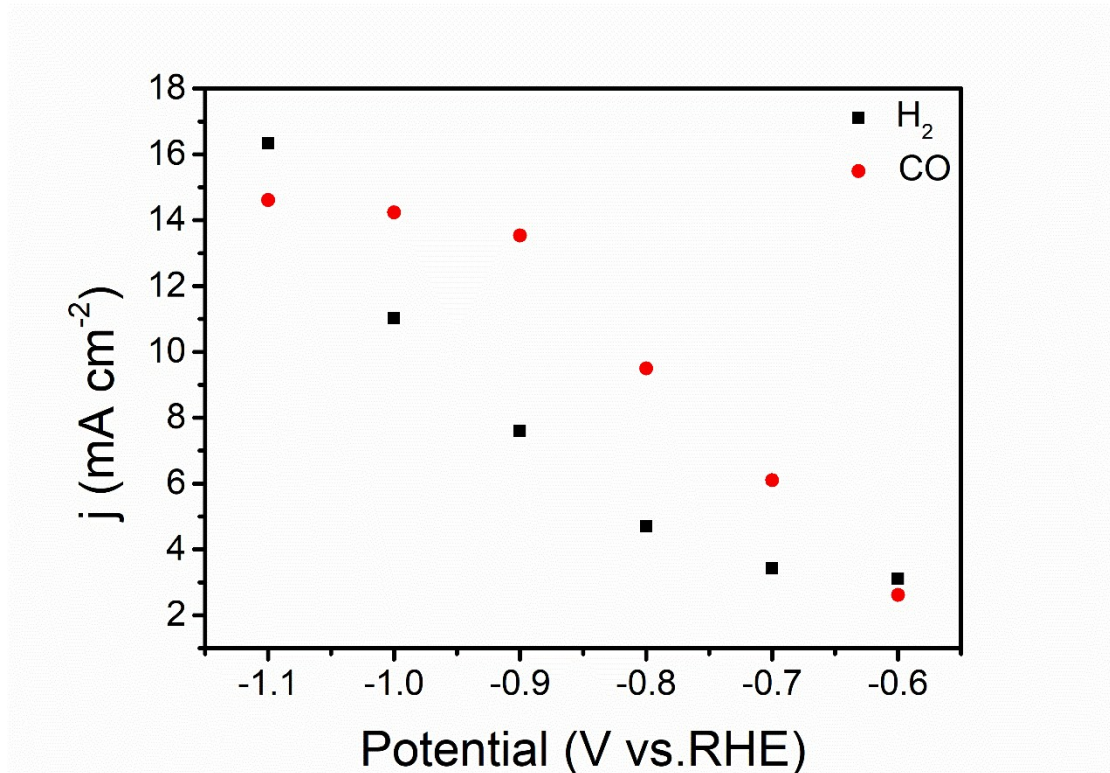


Fig. S12. Partial current density of CO and H_2 over nanoporous Au under different overpotentials.

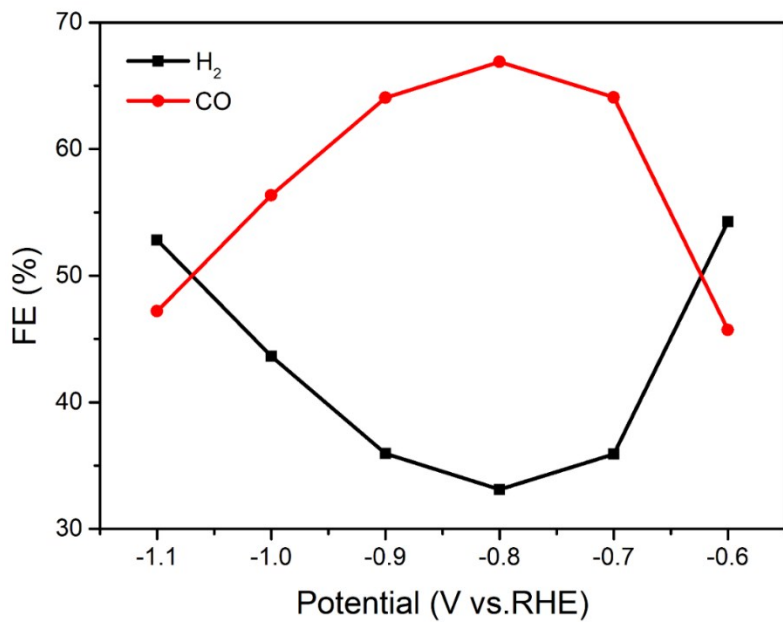


Fig. S13. Electrochemical CO₂ reduction activity on nanoporous Au.

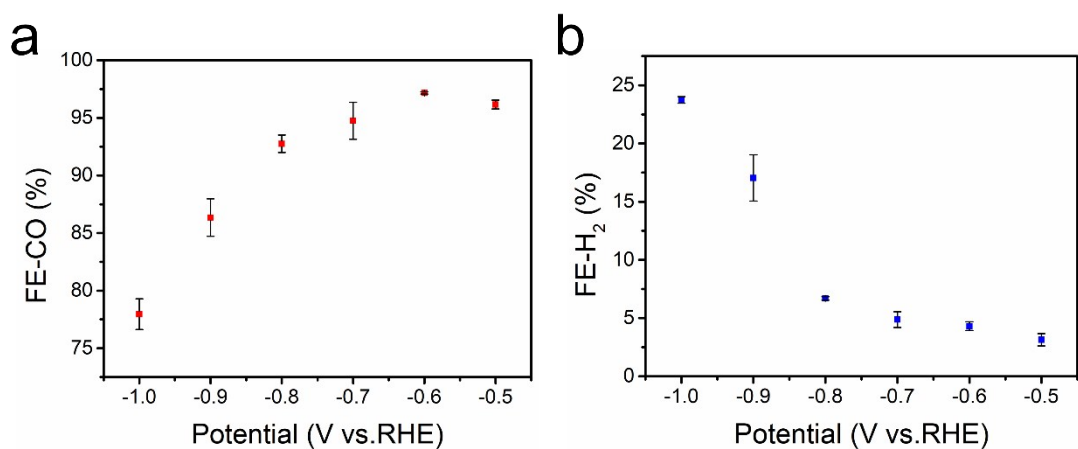


Fig. S14. Error-bar plots of FE for production of CO and H₂ over nanoporous AuCu₃@Au at different potentials.

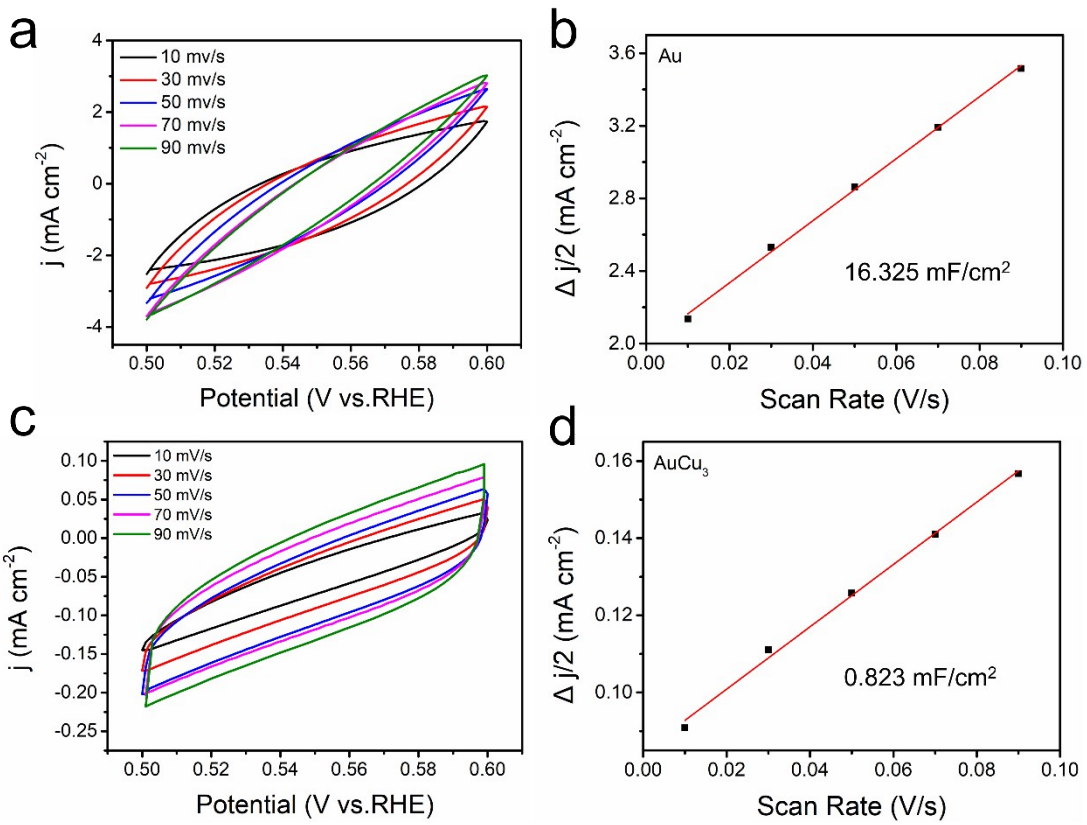


Fig. S15. Electrochemical double layer capacitance (EDLC) of nanoporous Au and nanoporous AuCu_3 @Au.

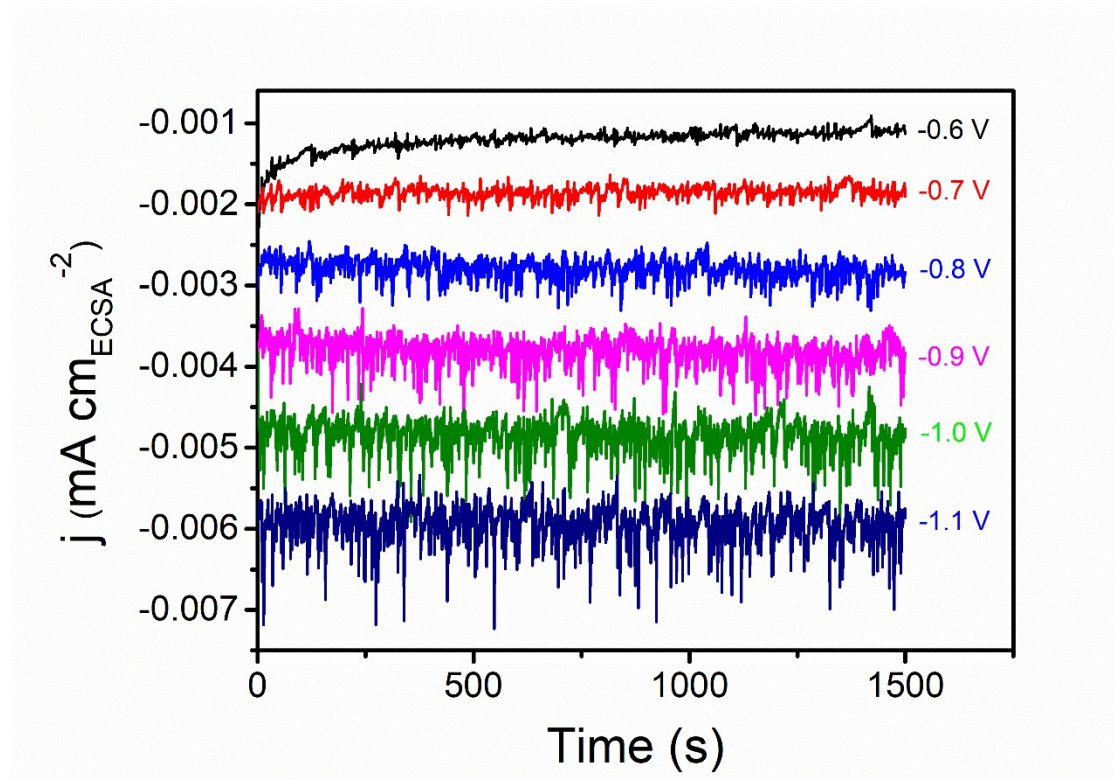


Fig. S16. Total current densities over nanoporous Au as a function of time at different potentials. At high overpotentials, the signals become noisy as a result of the intense gas evolution fluctuated.

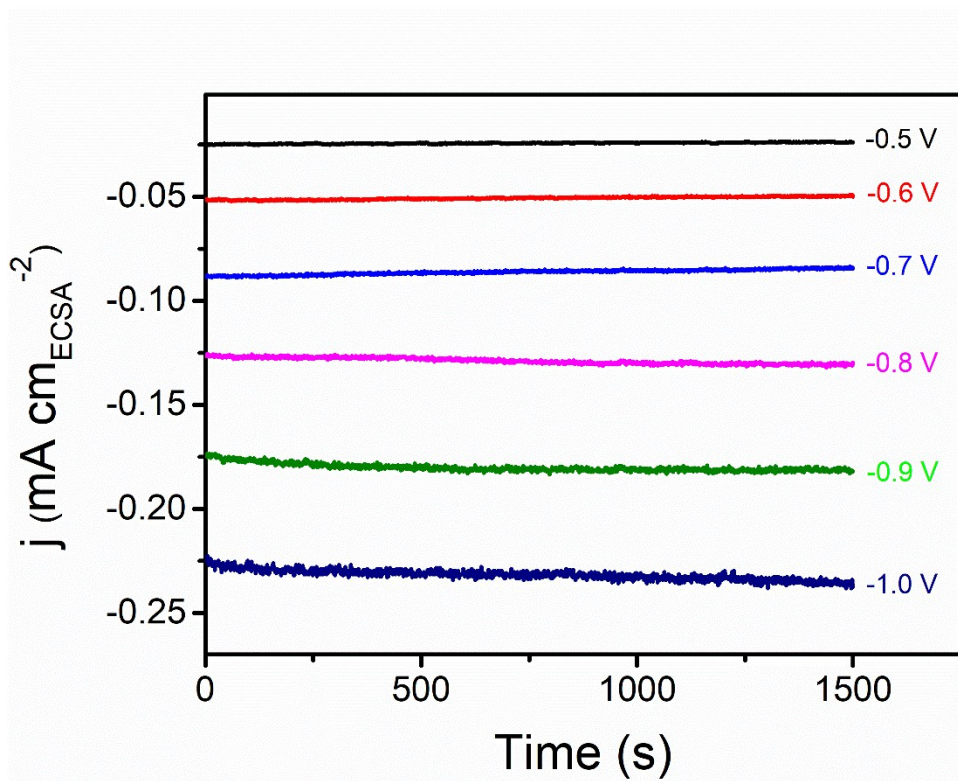


Fig. S17. Total current densities for $\text{AuCu}_3@\text{Au}$ as a function of time at different potentials, showing that the signals are clearer than those of nanoporous Au at high potentials.

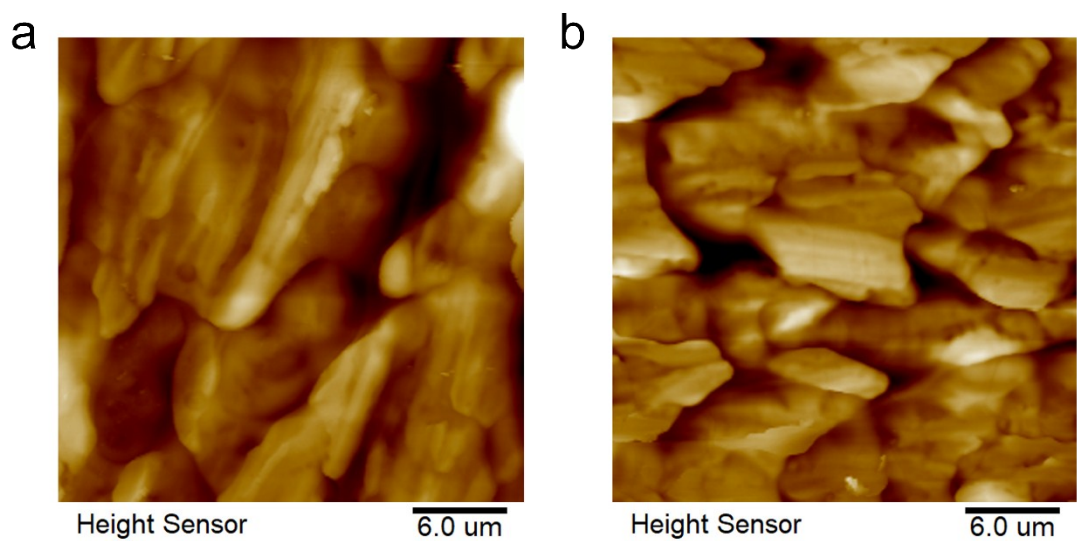


Fig. S18. AFM images of (a) nanoporous Au, Rq is 348nm (b) nanoporous AuCu_3 , Rq is 292nm.

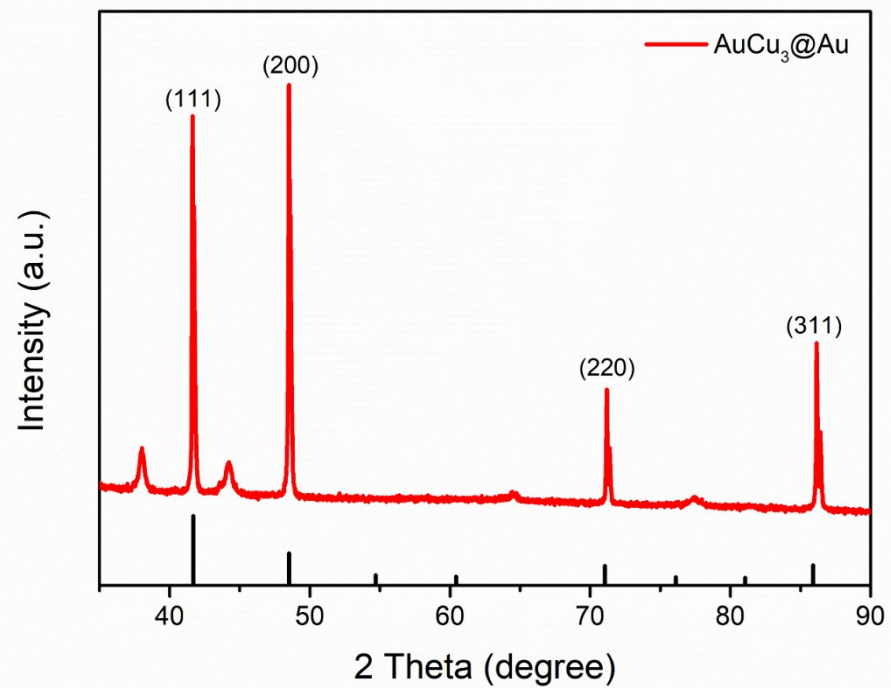


Fig. S19. XRD pattern of nanoporous monolithic $\text{AuCu}_3@\text{Au}$ electrode after CO_2 RR test.

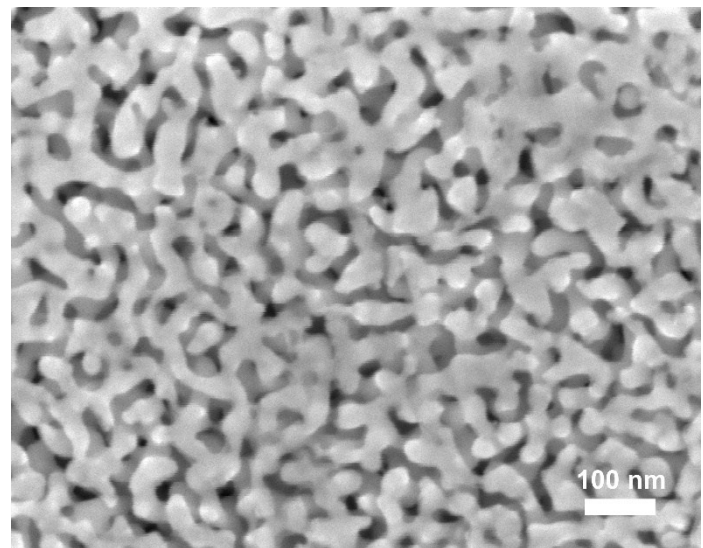


Fig. S20. SEM image of nanoporous $\text{AuCu}_3@\text{Au}$ after the catalytic CO_2 RR.

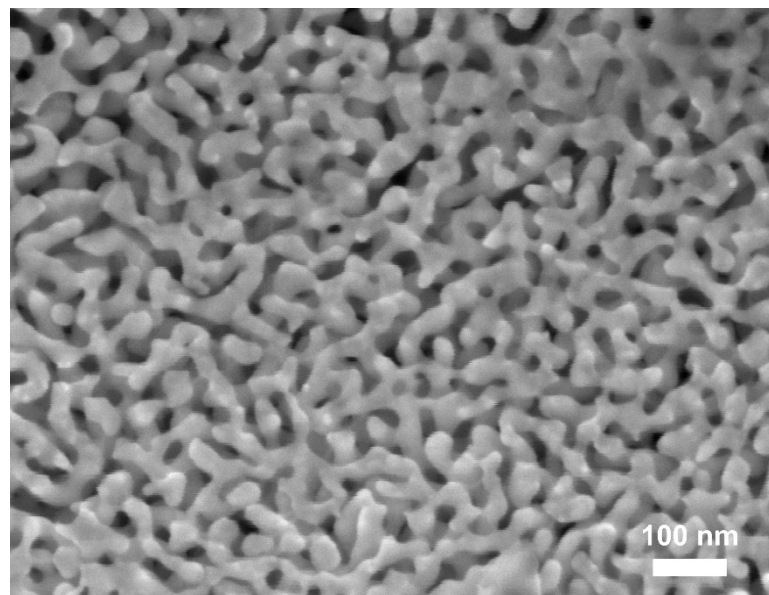


Fig. S21. SEM image of nanoporous $\text{AuCu}_3@\text{Au}$ after 100 h of electrocatalytic test.

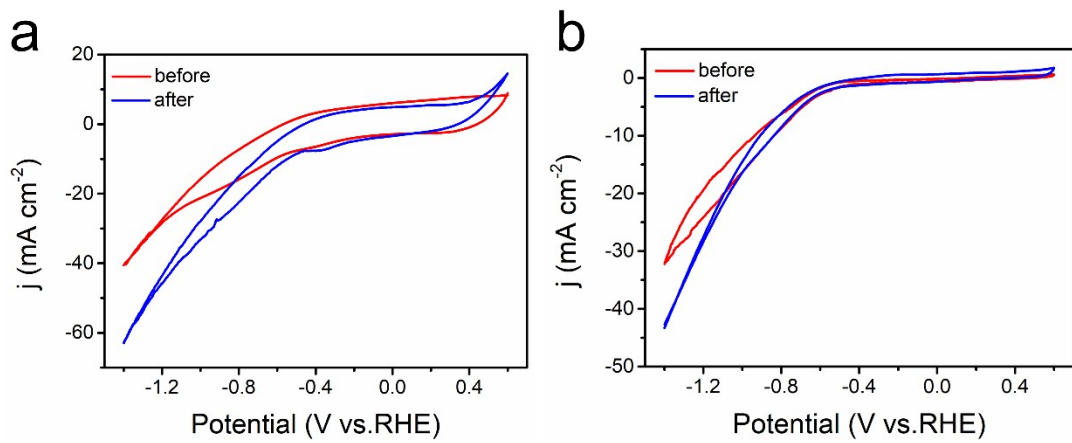


Fig. S22. CVs of (a) nanoporous Au, (b) nanoporous $\text{AuCu}_3@\text{Au}$ before and after electrochemical tests

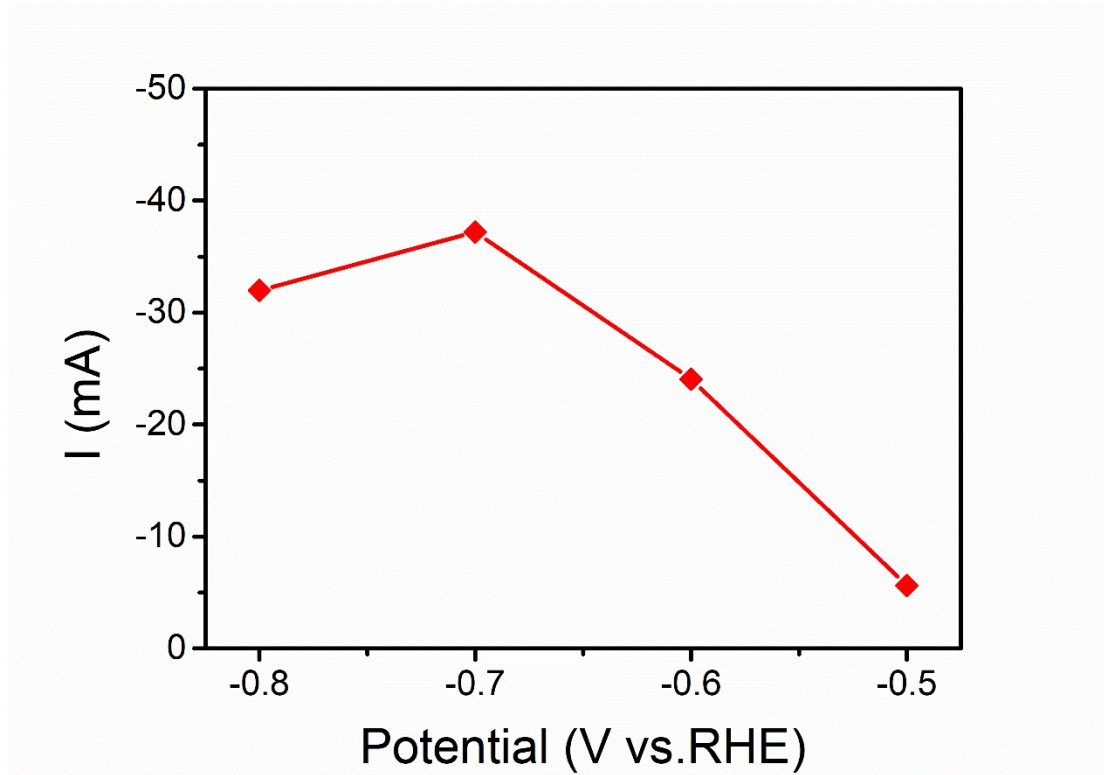


Fig. S23. Current of 23 cm-long nano-porous $\text{AuCu}_3@\text{Au}$ bulk electrode at different potentials.

Table S1. Au L₃-edge and Cu k-edge EXAFS fitting results (R : distance; CN: coordination number; σ^2 : Debye-Waller factor; ΔE_0 : inner potential correction) of $\text{AuCu}_3@\text{Au}$ sample.

Edge	Au-Au/Cu-Cu		Au-Cu/Cu-Au		σ^2 (\AA^2)	ΔE_0 (eV)
	R (\AA)	CN	R (\AA)	CN		
Au L ₃	2.86 \pm 0.01	7.6 \pm 0.8			0.0082 \pm 0.0007(Au)	4.5 \pm 0.7
Cu K	2.58 \pm 0.01	4.7 \pm 0.4	2.63 \pm 0.02	0.6 \pm 0.2	0.0096 \pm 0.0007(Cu)	2.9 \pm 0.9

Table S2. The comparisons with the reported metal-based electrocatalysts for CO₂ reduction.

Catalysts	Electrolyte	Potential (V vs.RHE)	CO average yield ($\mu\text{mol h}^{-1}$)	CO partial current density (mA cm^{-2})	Faradaic efficiency (%)	References
Tri-Ag-NPs	0.1M KHCO ₃	-0.855	23.3	1.25	96.8	[3]
Au NWs	0.5M KHCO ₃	-0.35	143.1	7.67	94	[4]
Pd NPs	0.1M KHCO ₃	-0.89	162.3	8.208	91.2	[5]
Zn dendrite	0.5M KHCO ₃	-1.1	261.2	10.27	79	[6]
Au _{0.87} Cu _{0.13}	0.1M KHCO ₃	-0.8	80.9	4.05	90	[7]
Ag@Cu	0.1M KHCO ₃	-1.06	38.2	2.5	82	[8]
CuIn	0.1M KHCO ₃	-0.7	29.6	1.62	95	[9]
CuPd	0.1M KHCO ₃	-0.9	58.8	3.2	87	[10]
Cu/SnO ₂	0.5M KHCO ₃	-0.7	79.8	11	93	[11]
AuCu₃@Au	0.5M KHCO₃	-0.6	203.6	5.3	97.3	This work

Notes and references

1. J. Kibsgaard and T. F. Jaramillo, *Angew. Chem. Int. Ed.* 2014, **53**, 14433–14437.
2. C. Y. Tang, W. Wang, A. K. Sun, C. K. Qi, D. Z. Zhang, Z. Z. Wu and D. Z. Wang, *ACS Catal.* 2015, **5**, 6956–6963.
3. S. Liu, H. Tao, L. Zeng, Q. Liu, Z. Xu, Q. Liu, J.-L. Luo, *J. Am. Chem. Soc.* 2017, **139**, 2160-2163.
4. W. Zhu, Y.J. Zhang, H. Zhang, H. Lv, Q. Li, R. Michalsky, A.A. Peterson, S. Sun, *J. Am. Chem. Soc.* 2014, **136**, 16132-16135.
5. D. Gao, H. Zhou, J. Wang, S. Miao, F. Yang, G. Wang, J. Wang, X. Bao, *J. Am. Chem. Soc.* 2015, **137**, 4288-4291.
6. J. Rosen, G.S. Hutchings, Q. Lu, R.V. Forest, A. Moore, F. Jiao, *ACS Catal.* 2015, **5**, 4586-4591.
7. C. Roy, J. Galipaud, L. Fréchette-Viens, S. Garbarino, J. Qiao, D. Guay, *Electrochim. Acta* 2017, **246**, 115-122.
8. Z. Chang, S. Huo, W. Zhang, J. Fang, H. Wang, *J. Phys. Chem. C* 2017, **121**, 11368-11379.
9. S. Rasul, D.H. Anjum, A. Jedidi, Y. Minenkov, L. Cavallo, K. Takanabe, *Angew. Chem. Int. Ed.* 2015, **54**, 2146-2150.
10. Y. Mun, S. Lee, A. Cho, S. Kim, J.W. Han, J. Lee, *Appl. Catal., B* 2019, **246**, 82-88.
11. Q. Li, J. Fu, W. Zhu, Z. Chen, B. Shen, L. Wu, Z. Xi, T. Wang, G. Lu, J.J. Zhu, S. Sun, *J. Am. Chem. Soc.* 2017, **139**, 4290-4293.